ISSN 2070-2051, Protection of Metals and Physical Chemistry of Surfaces, 2024, Vol. 60, No. 6, pp. 1050–1063. © Pleiades Publishing, Ltd., 2024.

NANOSCALE AND NANOSTRUCTURED MATERIALS AND COATINGS

Investigating the Treatment of Transition Metals for Ameliorating the Ability of Boron Nitride for Gas Sensing & Removing: A Molecular Characterization by DFT Framework

Fatemeh Mollaamin*

Department of Biomedical Engineering, Faculty of Engineering and Architecture, Kastamonu University, Kastamonu, 37210 Turkey

**e-mail: smollaamin@gmail.com*

Received December 29, 2023; revised April 24, 2024; accepted May 15, 2024

Abstract—The electronic, magnetic and thermodynamic properties of adsorption of toxic gases including NO molecules by using transition metals of *X* (*X* = Sc, V, Cr, Co, Cu, Zn)-doped boron nitride nanocage (B_5N_{10}_NC) have been investigated using density functional theory. The results denote that NO@*X*–B_4N_{10}_NC are stable compounds, with the most stable adsorption site being the center of the cage ring. The partial density of states (PDOS) can evaluate a determined charge assembly between gas molecules and *X*–B_4N_{10}_NC which indicates the competition among dominant complexes of Sc, V, Cr, Co, Cu, Zn. Based on NQR analysis, *X*-doped on B_5N_{10}_NC has shown the lowest fluctuation in electric potential and the highest negative atomic charge including 0.3710 C (copper), 0.5970 C (chromium), 0.7392 C (vanadium), 0.7768 C (zinc) and 0.8259 C (scandium), respectively, have presented the most tendency for being the electron acceptors. Furthermore, the reported results of NMR spectroscopy have exhibited that the yield of electron accepting for doping atoms on the *X*–B_4N_{10}_NC through gas molecules adsorption can be ordered as: Co ≈ Cr > Cu > Zn > V ≈ SC that exhibits the strength of covalent bond between scandium, vanadium, chromium, cobalt, copper, zinc and NO towards toxic gas removal from air. In fact, the adsorption of NO gas molecules can introduce spin polarization on the *X*–B_4N_{10}_NC which specifies that these surfaces may be employed as magnetic scavenging surface as a gas detector. Regarding IR spectroscopy, doped nanocages of Sc–B_4N_{10}_NC, V–B_4N_{10}_NC, Cr–B_4N_{10}_NC, Co–B_4N_{10}_NC, Cu–B_4N_{10}_NC and Zn–B_4N_{10}_NC, respectively, have the most fluctuations and the highest adsorption tendency for gas molecules which can address specific questions on the individual effect of charge carriers (gas molecule-nanocage), as well as doping atoms on the overall structure. Based on the results of ΔG_R° amounts in this research, the maximum efficiency of Sc, V, Cr, Co, Cu, Zn atoms doping of B_5N_{10}_NC for gas molecules adsorption depends on the covalent bond between NO molecules and *X*–B_4N_{10}_NC as a potent sensor for air pollution removal. Finally, high selectivity of atom-doped on boron nitride nanocage (gas sensor) for gas molecules adsorption has been resulted as: Cu ⩾ Co > Cr > V > Zn > Sc.

Keywords: environmental pollution, gas detecting, nanomaterials, transition metals, DFT

DOI: 10.1134/S2070205124702502

1. INTRODUCTION

Boron nitride nanomaterials have been used owing to their unparalleled specifications of eco-friendly attributes for pollutant adsorption and semiconducting property [1–4].

Boron nitride nanometerials usually exhibits semileading behavior, which is considered a proper alternative to carbon nanotubes. The properties of boron and nitrogen atoms which are the first neighbors of carbon in the periodic table, make boron nitride as an interesting subject of numerous studies [5–7].

In recent years, different investigations on the adsorption of chemical contaminants and applying various boron nitride nanostructures as adsorbents for water purification have been studied [8–10].

Various physical shapes of boron nitride (BN)-based nano adsorbents such as nanoparticles, fullerenes, nanotubes, nanofibers, nanoribbons, nanosheets, nanomeshes, nanoflowers, and hollow spheres have been broadly considered possible adsorbents owing to their exceptional characteristics such as large surface area, structural variability, great chemical/mechanical strength, abundant structural defects, high reactive sites, and functional groups [11, 12].

Adsorption involving charged adsorbates causes a change in the double layer and the potential at the outer Helmholtz plane, influencing the adsorption

rates of both anodic and cathodic reactions. The first three modes are intimately with adsorption and the double layer involves interaction of the adsorbates and the intermediate products. These compounds have been formed during the partial electrochemical reactions and interaction of the adsorbed intermediates with organic molecules which can either inhibit or enhance electrode reaction rate.

Particularly, this research work aims to assess the influences of doping atoms of Sc, V, Cr, Co, Cu, Zn on the B_5N_{10}_NC for increasing gas detection through measurement of some parameters containing charge transfer, electric potential, electromagnetic and thermodynamic properties, surface area, functional group and examine the removal of selected toxic gas molecules including nitrogen monoxide during adsorption process.

2. THEORETICAL INSIGHTS, APPLIED MATERIAL AND METHOD

2.1. NO Molecules Adsorption on X–B_4N_{10}_NC

The aim of this study is to remove toxic gas molecules including NO from air through an eco-friendly approach by using (Sc, V, Cr, Co, Cu, Zn)-doped B_5N_{10}_NC (Fig. 1).

Boron nitride nanocage was modeled in the presence of doping atoms of scandium, vanadium, chromium, cobalt, copper and zinc which can increase the gas sensing potential of BN-nanocage. In our research, sample characterization was performed by CAM–B3LYP–D3/EPR-3, LANL2DZ level of theory.

Figure 1 has shown the process of NO adsorption on the *X*–B_4N_{10}_NC surface which towards formation of complexes containing NO@Sc–B_4N_{10}_NC, NO@V–B_4N_{10}_NC, NO@Cr–B_4N_{10}_NC, NO@Co–B_4N_{10}_NC, NO@Cu–B_4N_{10}_NC, NO@Zn–B_4N_{10}_NC by molecular modeling computations.

The charge distribution of mentioned complexes is calculated due to the Bader charge analysis [13].

The trapping of NO molecules by *X*–B_4N_{10}_NC (*X* = Sc, V, Cr, Co, Cu, Zn) were successfully incorporated due to binding formation consisting of N → Sc, N → V, N → Cr, N → Co, N → Cu, N → Zn (Fig.1).

2.2. Application of Density Functional Theory Approach

Hohenberg–Kohn (HK) functions have rigidly made the electronic density permissible as fundamental variable to electronic and structure computations. In other words, development of the applied density functional theory (DFT) methodology only became notable after W. Kohn and L. J. Sham released their reputable series of equations which are introduced as Kohn–Sham (KS) equations [14–19].

Considering the electronic density within the KS image directs us to a remarkable reduction of quantum computing. Thus, the KS methodology lightens the route for pursuing systems that cannot be discussed by conventional ab-initio methodologies. Kohn and Sham introduces the solution which brings up the mono-electronic orbitals to account the kinetic energy in a simple and relatively exact, by finding a residual modification that might be computed apart. So, one starts with a reference model of *M* with non-interacting electrons related to the external potential v_s and with Hamiltonian [18, 19]:

$$\hat{H}_s = -\sum_i^M \frac{1}{2}\bar{\nabla}_i^2 + \sum_i^M v_s(\vec{r}_i) = \sum_i^M \hat{h}_s;$$
$$\hat{h}_s = -\frac{1}{2}\bar{\nabla}_i^2 + v_s(\vec{r}_i). \quad (1)$$

By representing the single particle orbitals ψ_i all electronic densities physically acceptable for the system of "non-interacting" electrons are written in the Eq. (2):

$$\rho(\vec{r}) = \sum_i^M |\psi_i(\vec{r})|^2. \quad (2)$$

Finally, the total energy could be measured by the KS method due to the Eq. (3):

$$E[\rho] = \sum_i^M n_i \psi_i \left| -\frac{1}{2}\bar{\nabla}^2 + v_{\text{ext}}(\vec{r}) + \frac{1}{2}\int \frac{\rho(\vec{r}')}{|\vec{r}-\vec{r}'|} d\vec{r}' \right| \psi_i + E_{\text{xc}}[\rho] + \frac{1}{2}\sum_\beta^N \sum_{\alpha\neq\beta}^N \frac{Z_\alpha Z_\beta}{|\vec{R}_\alpha - \vec{R}_\beta|}. \quad (3)$$

Therefore, the precise exchange energy functional is described by the Kohn–Sham orbitals in lieu of the density which is cited as the indirect density functional. This research has employed the penetration of the hybrid functional of three-parameter basis set of B3LYP (Becke, Lee, Yang, Parr) within the conception of DFT upon theoretical computations [20, 21]. The popular B3LYP (Becke, three-parameter, Lee–Yang–Parr) and exchange-correlation functional becomes based on Eq. (4) [22–24]:

$$E_{\text{XC}}^{\text{B3LYP}} = (1-\alpha)E_{\text{x}}^{\text{LSDA}} + \alpha E_{\text{x}}^{\text{HF}} + bE_{\text{x}}^{\text{B}} + (1-c)E_{\text{c}}^{\text{LSDA}} + cE_{\text{c}}^{\text{LYP}}, \quad (4)$$

$\alpha = 0.20$, $b = 0.72$, $c = 0.81$ shows a generalized gradient approximation: the Becke ex-change functional [25] and the correlation functional of Lee, Yang and Parr [26] for B3LYP and $E_{\text{c}}^{\text{LSDA}}$ is the VWN local spin density approximation to the correlation functional [27].

In this article, the rigid PES using DFT calculations have been computed applying Gaussian 16 revision C.01 software [28]. The input Z-matrix for adsorption of NO molecules in air by the *X*–

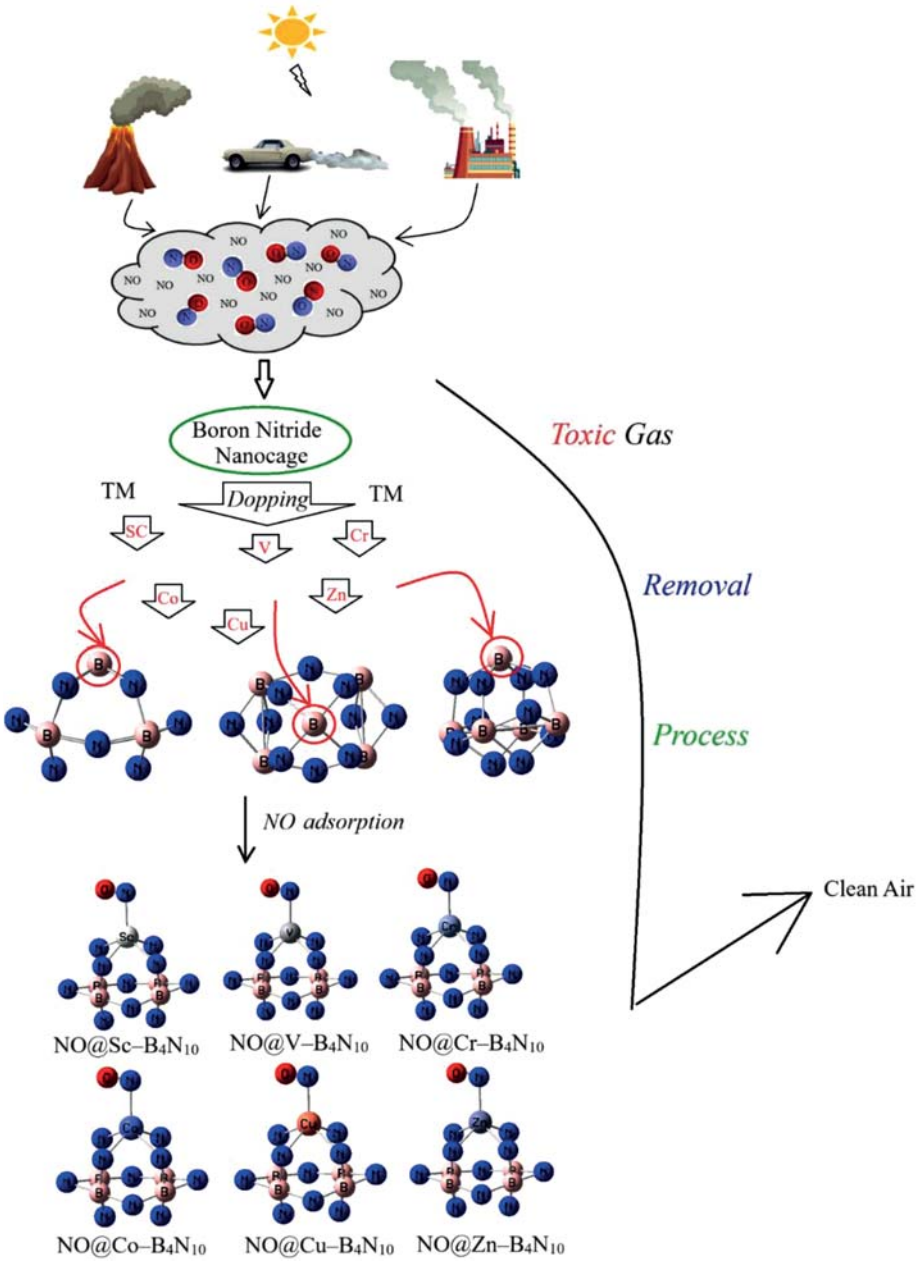

Fig. 1. Application of X–B_4N_{10}_NC towards adsorption of gas molecules of NO and formation of complexes: NO@Sc–B_4N_{10}_NC, NO@V–B_4N_{10}_NC, NO@Cr–B_4N_{10}_NC, NO@Co–B_4N_{10}_NC, NO@Cu–B_4N_{10}_NC, NO@Zn–B_4N_{10}_NC complexes using CAM–B3LYP-D3/6–311+G(d,p), LANL2DZ calculation. The sign of adsorption is shown with @.

B_4N_{10}_NC has been designed with GaussView 6.1 [29] using 6-311+G(d,p), EPR-3, LANL2DZ basis set. In this study, the interaction between gas molecules and X–B_4N_{10}_NC was modeled and analyzed. As revealed by DFT-based analysis, the potency of X–B_4N_{10}_NC for grabbing NO molecules was determined mainly by the electronegativity of the functional groups, as well as the interaction between the X–B_4N_{10}_NC and the NO molecules.

3. RESULTS AND DISCUSSION

One of the most dominant gas pollutants in the air is nitrogen monoxide. The data has evaluated the efficiency of boron nitride nanocage doped with Sc, V, Cr, Co, Cu, Zn for gas detection. In fact, it can be remarked the chemisorptive nature of the bond among the gas molecules with boron and nitrogen elements through the equilibrium distribution of doping atoms, B_5N_{10}_NC, and a monolayer attribute.

3.1. PDOS & Electronic Evaluating

The electronic structures of NO adsorption using *X* (*X* = Sc, V, Cr, Co, Cu, Zn)-doped B_5N_{10}_NC as the selective sensor for detecting and grabbing gas molecules in the air have been illustrated using CAM–B3LYP–D3/6-311+G(d,p), LANL2DZ level of theory.

Figures 2a–2f shows the projected density of state (PDOS) of NO@*X*–B_4N_{10}_NC through gas molecules adsorption. The appearance of the energy states (*p*-orbital) of N, O and (*d*-orbital) of Sc, V, Cr, Co, Cu, Zn within the gap of *X*–B_4N_{10}_NC induces the reactivity of the system. It is clear from the figure that after trapping with gas molecules, there is a significant contribution of *d*-orbital in the unoccupied level. Therefore, the curve of partial PDOS has described that the *p* states of N atoms in gas molecules and *d*-orbital in Sc, V, Cr, Co, Cu, Zn transition metals in *X*–B_4N_{10}_NC overcome due to the conduction band (Figs. 2a–2f). A distinguished adsorption trait might be seen in NO@*X*–B_4N_{10}_NC because of the potent interaction between the *p* states of nitrogen atom in gas molecules with *d* states of Sc, V, Cr, Co, Cu, Zn in *X*–B_4N_{10}_NC complexes.

Figures 2a–2f shows that NO@Sc–B_4N_{10}_NC, NO@V–B_4N_{10}_NC, NO@Cr–B_4N_{10}_NC, NO@Co–B_4N_{10}_NC, NO@Cu–B_4N_{10}_NC, and NO@Zn–B_4N_{10}_NC complexes through gas molecules adsorption, respectively, have the most contribution at the middle of the conduction band between −5 to −15 eV, while contribution of boron and nitrogen states are enlarged and similar together, and adsorbing of NO depicts interfacial electronic of the B_4N_{10}_NC for selection of this gas. NO@Sc–B_4N_{10}_NC has indicated one sharp peak around −12.5 eV for Sc in Fig. 2a, while NO@V–B_4N_{10}_NC (Fig. 2b) and NO@Cr–B_4N_{10}_NC complexes (Fig. 2c) have exhibited two sharp peaks around −10 and −14.5 eV for V and Cr atoms, respectively. Furthermore, NO@Co–B_4N_{10}_NC (Fig. 2d) has exhibited four strong peaks around −8, −10, −11.5 and −14.5 eV through the graphs for Co atom. Furthermore, the Cu graph with two sharp close peaks around −14 and −14.5 eV in NO@Cu–B_4N_{10}_NC (Fig. 2e) has been shown. However, Zn graph in NO@Zn–B_4N_{10}_NC (Fig. 2f) with a sharp peak around −19.5 eV attracts our attention. Therefore, the order potency of gas adsorption by doping atoms of Sc, V, Cr, Co, Cu, Zn on *X*–B_4N_{10}_NC based on the PDOS might be shifted as: Cu–B_4N_{10}_NC ⩾ Co–B_4N_{10}_NC > Cr–B_4N_{10}_NC > V–B_4N_{10}_NC > Zn–B_4N_{10}_NC > Sc–B_4N_{10}_NC.

3.2. Insight to Nuclear Quadrupole Resonance

As the electric field gradient (EFG) at the citation of the nucleus in NO is allocated by the valence electrons twisted in the attachment with close nuclei of *X*–B_4N_{10}_NC through trapping of gas molecules, the nuclear quadrupole resonance (NQR) frequency at which transitions occur is particular for NO@*X*–B_4N_{10}_NC complexes (Table1). The NQR method is related to the multipole expansion in Cartesian coordinates as the Eq. (5) [30, 31]:

$$V(r) = V(0) + \left[\left(\frac{\partial V}{\partial x_i}\right)_0 x_i\right] + \frac{1}{2}\left[\left(\frac{\partial^2 V}{\partial x_i x_j}\right)_0 x_i x_j\right] + \ldots . \quad (5)$$

After that, a simplification on the Eq. (5), there are only the second derivatives related to the identical variable for the potential energy [30, 31]:

$$\begin{aligned} U &= -\frac{1}{2}\int_{\mathcal{D}} d^3 r \rho_r \left[\left(\frac{\partial^2 V}{\partial x_i^2}\right)_0 x_i^2\right] \\ &= -\frac{1}{2}\int_{\mathcal{D}} d^3 r \rho_r \left[\left(\frac{\partial E_i}{\partial x_i}\right)_0 x_i^2\right] \\ &= -\frac{1}{2}\left(\frac{\partial E_i}{\partial x_i}\right)_0 \int_{\mathcal{D}} d^3 r \left[\rho(r) x_i^2\right]. \end{aligned} \quad (6)$$

There are two parameters which must be gotten from NQR experiments: the quadrupole coupling constant, χ, and asymmetry parameter of the EFG tensor η:

$$\chi = e^2 Q q_{zz}/h , \quad (7)$$

$$\eta = q_{xx} - q_{yy}/q_{zz} , \quad (8)$$

where q_{ii} are ingredients of the EFG tensor at the quadrupole nucleus determined in the EFG principal axes system, *Q* is the nuclear quadrupole moment, *e* is the proton charge and *h* is the Planck's constant [32, 33].

In this research work, the electric potential as the quantity of work energy through carrying over the electric charge from one position to another position in the essence of electric field has been evaluated for NO@Sc–B_4N_{10}_NC, NO@V–B_4N_{10}_NC, NO@Cr–B_4N_{10}_NC, NO@Co–B_4N_{10}_NC, NO@Cu–B_4N_{10}_NC, and NO@Zn–B_4N_{10}_NC complexes (Table 1).

In Table 1, the Bader charge and electronic potential properties of Sc, V, Cr, Co, Cu, Zn and B, N in *X*–B_4N_{10}_NC and N, O of NO molecules trapped on doped-boron nitride nanocages have been investigated. The amounts indicate that with increasing the negative charge of different atoms, the electric potential resulted from NQR calculations increase. Moreover, the doping atoms of Sc (15), V(15), Cr(15), Co(15), Cu(15), Zn(15) on the B_5N_{10}_NC have shown the most potential for accepting the electron from electron donor of N(1) and O (2) in NO adsorbed on the *X*–B_4N_{10}_NC (Table 1).

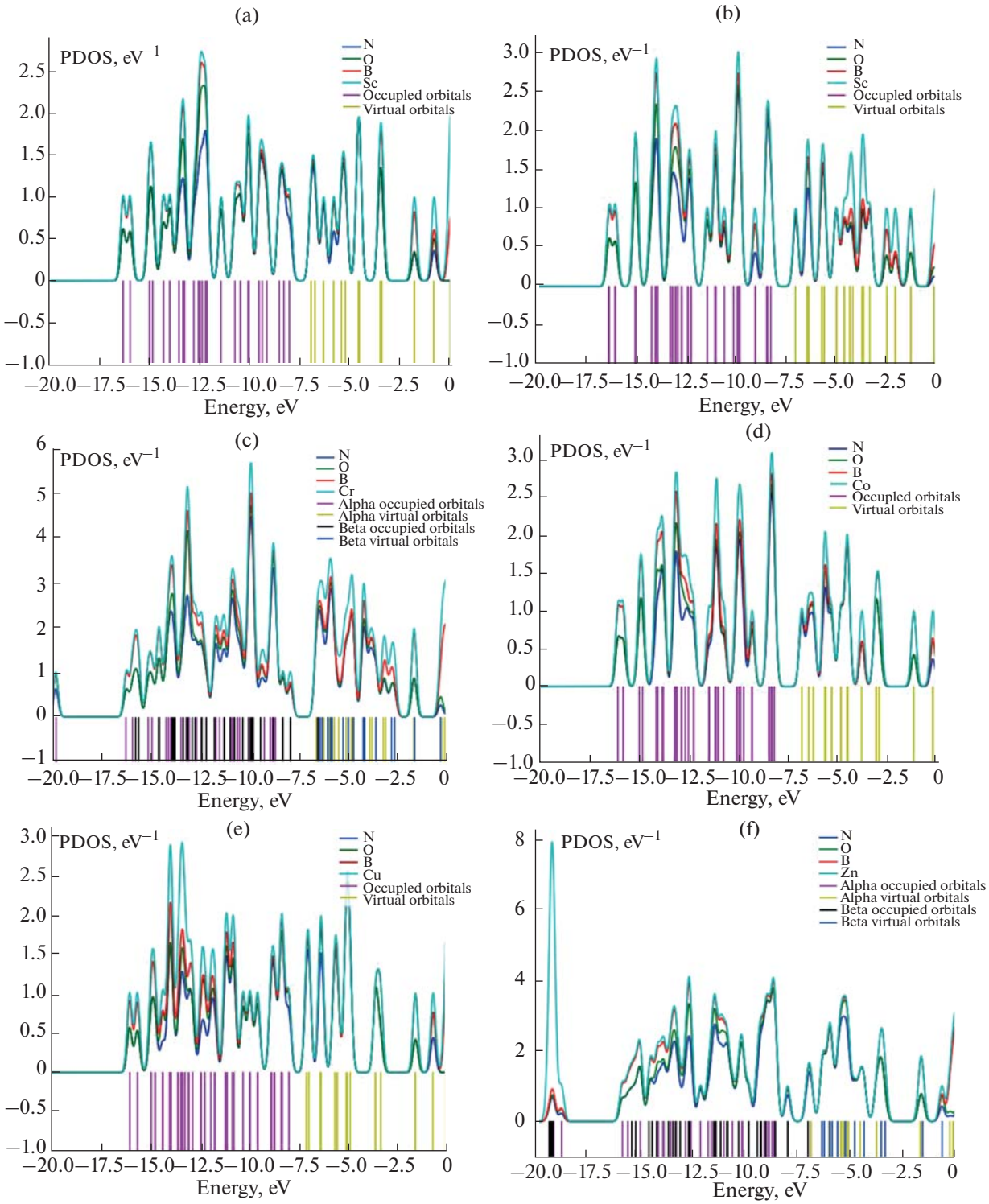

Fig. 2. PDOS of gas molecules of NO adsorbed on *X*–B_4N_{10}_NC including (a) NO@Sc–B_4N_{10}_NC, (b) NO@V–B_4N_{10}_NC, (c) NO@Cr–B_4N_{10}_NC, (d) NO@Co–B_4N_{10}_NC, (e) NO@ Cu–B_4N_{10}_NC, and (f) NO@Zn–B_4N_{10}_NC complexes by CAM–B3LYP–D3/6-311+G(d,p), LANL2DZ.

Furthermore, in Figs. 3a–3f, it has been sketched the electric potential of nuclear quadrupole resonance for some atoms of Sc, V, Cr, Co, Cu, Zn/B, N in *X*–B_4N_{10}_NC and N, O of gas molecules trapped on doped-boron nitride nanocages which has been calculated by CAM–B3LYP–D3/EPR-3, LANL2DZ.

Table 1. The electric potential (arb. units) and Bader charge (e) through NQR calculation for NO@Sc–B_4N_{10}_NC, NO@V–B_4N_{10}_NC, NO@Cr–B_4N_{10}_NC, NO@Co–B_4N_{10}_NC, NO@Cu–B_4N_{10}_NC, and NO@Zn–B_4N_{10}_NC complexes using CAM–B3LYP–D3/EPR-3, LANL2DZ calculation

Sc–B_4N_{10}_NC			V–B_4N_{10}_NC			Cr–B_4N_{10}_NC		
Atom	Q	E_p	Atom	Q	E_p	Atom	Q	E_p
N1	–0.0623	–18.2437	N1	–0.0365	–18.2092	N1	–0.1006	–18.2437
O2	–0.1170	–22.1969	O2	–0.1158	–22.195	O2	–0.0957	–22.2099
B3	0.0990	–11.2667	B3	0.1395	–11.2682	B3	0.1151	–11.2746
N4	0.0053	–18.2607	N4	–0.0462	–18.2769	N4	–0.0326	–18.2739
N5	–0.0532	–18.2476	N5	–0.0743	–18.2656	N5	–0.0825	–18.2753
B6	0.1582	–11.2709	B6	0.1565	–11.2691	B6	0.1111	–11.2739
B7	0.0999	–11.2692	B7	0.1318	–11.2666	B7	0.1199	–11.2748
B8	0.1432	–11.2719	B8	0.1556	–11.2696	B8	0.1163	–11.2758
N9	–0.0445	–18.2559	N9	–0.0484	–18.2585	N9	–0.0326	–18.2658
N10	–0.0468	–18.2475	N10	–0.0737	–18.2644	N10	–0.0994	–18.2819
N11	–0.2326	–18.2756	N11	–0.2011	–18.2673	N11	–0.1406	–18.2638
N12	–0.2691	–18.2969	N12	–0.2187	–18.2679	N12	–0.1407	–18.2624
N13	–0.2051	–18.2834	N13	–0.1890	–18.2653	N13	–0.1347	–18.2608
N14	–0.2688	–18.2974	N14	–0.2199	–18.2674	N14	–0.1442	–18.2639
Sc15	0.8259	–9.3807	V15	0.7392	–12.4983	Cr15	0.5970	–14.3934
N16	–0.0267	–18.2483	N16	–0.0555	–18.2612	N16	–0.0291	–18.2635
N17	–0.0053	–18.2639	N17	–0.0432	–18.2744	N17	–0.0265	–18.2683
Co–B_4N_{10}_NC			Cu–B_4N_{10}_NC			Zn–B_4N_{10}_NC		
Atom	Q	E_p	Atom	Q	E_p	Atom	Q	E_p
O2	–0.1111	–22.1930	O2	–0.0847	–22.1827	O2	–0.0987	–22.1976
B3	0.1511	–11.2799	B3	0.1439	–11.2831	B3	0.1150	–11.2782
N4	–0.0547	–18.2763	N4	–0.0320	–18.2747	N4	–0.0185	–18.2727
N5	–0.0626	–18.2520	N5	–0.0657	–18.2511	N5	–0.0436	–18.2528
B6	0.1449	–11.2800	B6	0.1362	–11.2829	B6	0.1141	–11.2787
B7	0.1460	–11.2798	B7	0.1301	–11.2822	B7	0.1127	–11.2786
B8	0.1462	–11.2809	B8	0.1247	–11.2809	B8	0.1128	–11.2786
N9	–0.0739	–18.2786	N9	–0.0631	–18.273	N9	–0.0645	–18.2693
N10	–0.0678	–18.2558	N10	–0.0536	–18.2432	N10	–0.0414	–18.25
N11	–0.1124	–18.2576	N11	–0.1440	–18.2666	N11	–0.2080	–18.2814
N12	–0.125	–18.2642	N12	–0.1344	–18.2611	N12	–0.2116	–18.2823
N13	–0.1081	–18.257	N13	–0.1352	–18.2648	N13	–0.2026	–18.2819
N14	–0.1174	–18.2619	N14	–0.1410	–18.2634	N14	–0.2102	–18.2826
Co15	0.2962	–21.0329	Cu15	0.3710	–26.0693	Zn15	0.7768	–16.175
N16	–0.0817	–18.2785	N16	–0.0604	–18.273	N16	–0.0642	–18.2689
N17	–0.0510	–18.2718	N17	–0.0294	–18.2757	N17	–0.0174	–18.2724
N1	0.0813	–18.1696	N1	0.0377	–18.1784	N1	–0.0503	–18.2247

In Figs. 3a and 3b, it was observed the behavior of NO adsorption on the Sc–B_4N_{10}_NC and NO@V–B_4N_{10}_NC, respectively, with the analogous high sensitivity based on relation coefficient of $R^2 = 0.9314$ and $R^2 = 0.9591$. Adsorption of NO on the Cr–B_4N_{10}_NC and Co–B_4N_{10}_NC in Figs. 3c and 3d, respectively, has illustrated the highest sensing of $R^2 = 0.9332$ and $R^2 = 0.9218$. In addition, Figs. 3e and 3f has resulted

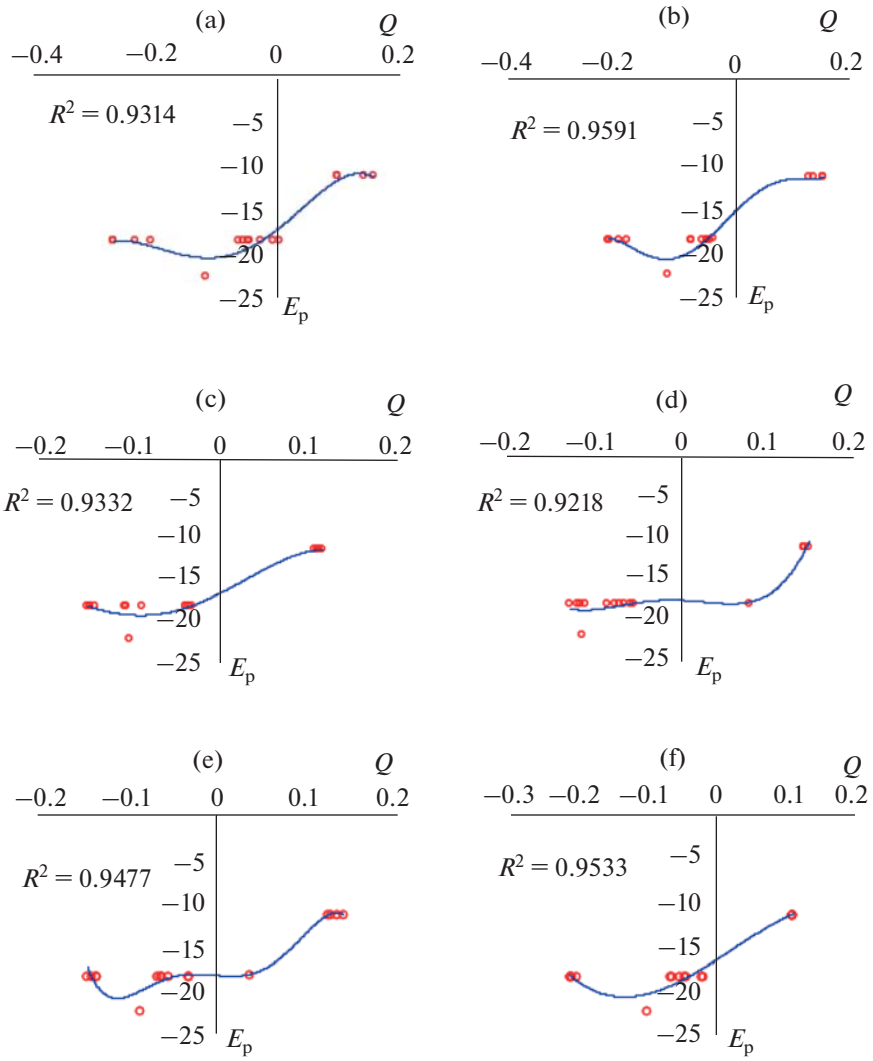

Fig. 3. Electric potential (arb. units) versus Bader charge (C) through NQR calculation for (a) NO@Sc–B_4N_{10}_NC, (b) NO@V–B_4N_{10}_NC, (c) NO@Cr–B_4N_{10}_NC, (d) NO@Co–B_4N_{10}_NC, (e) NO@Cu–B_4N_{10}_NC, and (f) NO@Zn–B_4N_{10}_NC complexes by CAM–B3LYP–D3/EPR-3, LANL2DZ.

that NO@Cu–B_4N_{10}_NC, and NO@Zn–B_4N_{10}_NC, respectively, has a good detecting for NO removal from air through relation coefficient of $R^2 = 0.9477$ and $R^2 = 0.9533$.

It's vivid that the curve of *X*–B_4N_{10}_NC is waved by NO molecules. The fluctuated peaks for electric potential have been shown around NO trapping on the *X*–B_4N_{10}_NC which demonstrate the electron accepting specifications of nitrogen and oxygen versus the scandium, vanadium, chromium, cobalt, copper and zinc doped on the B_4N_{10}_NC (Figs. 3a–3f). Besides, it can be considered that transitions metals as ferromagnetic semiconductors in the functionalized B_4N_{10}_NC might have more impressive sensitivity for accepting the electrons from NO by Sc, V, Cr, Co, Cu, Zn in the process of adsorption mechanism.

Table 1 has shown that cobalt-doped on B_5N_{10}_NC has the lowest fluctuation between Bader charge versus electric potential extract from NQR parameters and the highest negative atomic charge including 0.2962 C in NO@Co–B_4N_{10}_NC which can be an appropriate option with the highest tendency for electron accepting in the adsorption current (Table 1). In addition, the adsorbents of copper with 0.3710 C, chromium with 0.5970 C, vanadium with 0.7392 C, zinc with 0.7768 C and scandium with 0.8259 C, respectively, have presented the most tendency for being the electron acceptors. In fact, the uptake of gas molecules has been known to be associated with *X*–B_4N_{10}_NC, indicating that the adsorbed NO molecules in the *X*-doped nanocage can be internalized through a different pathway from pristine nanocage.

3.3. Analysis of Nuclear Magnetic Resonance Spectra

Based on resulted amounts, nuclear magnetic resonance (NMR) spectra of X–B_4N_{10}_NC (X = Sc, V, Cr, Co, Cu, Zn) as the potent sensor for adsorbing toxic gas molecules of NO can unravel the efficiency of X–B_4N_{10}_NC for detecting and removing of these hazardous gases in air as an ecofriendly approach.

From the DFT calculations, it has been attained the chemical shielding (CS) tensors in the principal axes system to estimate the isotropic chemical-shielding (CSI) and anisotropic chemical-shielding (CSA) [34]:

$$\sigma_{iso} = (\sigma_{11} + \sigma_{22} + \sigma_{33})/3, \quad (9)$$

$$\sigma_{aniso} = \sigma_{33} - (\sigma_{22} + \sigma_{11})/2. \quad (10)$$

The NMR data of isotropic (σ_{iso}) and anisotropic shielding tensors (σ_{aniso}) of gas molecules trapped in the X–B_4N_{10}_NC towards formation of NO@Sc–B_4N_{10}_NC, NO@V–B_4N_{10}_NC, NO@Cr–B_4N_{10}_NC, NO@Co–B_4N_{10}_NC, NO@Cu–B_4N_{10}_NC, and NO@Zn–B_4N_{10}_NC complexes have been computed by Gaussian 16 revision C.01 program package [28] and been shown in Table 2.

In Table 2, NMR data has reported the notable amounts for NO which were adsorbed on the X–B_4N_{10}_NC as the selective sensor for detecting gas molecules in air. The observed increase in the chemical shift anisotropy spans for N (1) and O (2) atoms of NO adsorption on the X–B_4N_{10}_NC. The observed weak signal intensity near the parallel edge of the nanocage pattern may be due to boron binding induced non-spherical distribution of these complexes.

It is remarkable that doping of Sc, V, Cr, Co, Cu, Zn on B_4N_{10}_NC might promote the stability of nanocage that results in enhanced magnetic alignment of complexes. Interestingly, the reported results show that Sc, V, Cr, Co, Cu, Zn elements can be optimized to achieve optimal alignment of nanocage in the presence of an applied magnetic field.

In fact, the adsorption of NO can introduce spin polarization on the X–B_4N_{10}_NC which indicates that these surfaces might be applied as magnetic scavenging surface as a gas detector. Isotropic and anisotropic shielding fluctuate with the occupancy in the electron accepting gas molecules trapped in the atom-doped on the boron nitride nanocage.

Figures 4a–4f exhibited the same tendency of shielding for boron and nitrogen; however, a considerable deviation exists from doping atoms of Sc (15), V (15), Cr (15), Co (15), Cu (15), Zn(15) through interaction with N (1) and O (2) of NO during adsorbing on the B_5N_{10}_NC.

In Figs. 4a–4f, gas molecules of NO in the complexes of NO@Sc–B_4N_{10}_NC (Fig. 4a), NO@V–B_4N_{10}_NC (Fig. 4b), NO@Cr–B_4N_{10}_NC (Fig. 4c), NO@Co–B_4N_{10}_NC (Fig. 4d), NO@Cu–B_4N_{10}_NC (Fig. 4e), and NO@Zn–B_4N_{10}_NC (Fig. 4f) denote the fluctuation in the chemical shielding during ion trapping.

Figures 4a–4f shows the gap chemical shielding between scandium, vanadium, chromium, cobalt, copper and zinc doping of X–B_4N_{10}_NC nanocage and NO gas molecules. The yield of electron accepting for doping atoms on the X–B_4N_{10}_NC through gas molecules adsorption can be ordered as: Co ≈ Cr > Cu > Zn > V ≈ SC that approves the possibility of covalent bond between scandium, vanadium, chromium, cobalt, copper, zinc and nitrogen monoxide towards removing it from the air.

In the NMR spectroscopy, it has been observed the remarkable peaks around interaction of NO molecules through adsorbing on the X–B_4N_{10}_NC during toxic gas detection and its scavenging from the air; however, there are some fluctuations in the chemical shielding behaviors of isotropic and anisotropy attributes.

Therefore, the authors believe that the extracted results would be useful in the design of X–B_4N_{10}_NC complexes based doped nanomaterials for increasing the adsorption of NO gas molecules in addition to the structural studies using solid-state and solution NMR techniques.

3.4. IR Spectroscopy and Thermodynamic Factors

The IR calculations have been accomplished for adsorption of NO molecules by X–B_4N_{10}_NC during toxic gas sensing in air. Therefore, it has been simulated the several clusters containing NO@Sc–B_4N_{10}_NC (Fig. 5a), NO@V–B_4N_{10}_NC (Fig. 5b), NO@ Cr–B_4N_{10}_NC (Fig. 5c), NO@Co–B_4N_{10}_NC (Fig. 5d), NO@Cu–B_4N_{10}_NC (Fig. 5e) and NO@Zn–B_4N_{10}_NC (Fig. 5f) complexes using CAM–B3LYP–D3/6-311+G(d,p), LANL2DZ.

The graph of Fig. 5a has been observed in the frequency range between 200–1200 cm^{-1} for NO@Sc–B_4N_{10}_NC with a sharp peak around 517.89 cm^{-1}. Figure 5b has shown the frequency range between 200–1100 cm^{-1} for NO@V–B_4N_{10}_NC with sharp peaks around 576.51, 585.20, and 666.98 cm^{-1}. Figure 5c has indicated the fluctuation of frequency between 100–1400 cm^{-1} for NO@Cr–B_4N_{10}_NC with several sharp peaks around 537.56, 547.52 and 1314.38 cm^{-1}. Figure 5d has shown the fluctuation of frequency between 100–1200 cm^{-1} for NO@Co–B_4N_{10}_NC with two sharp peaks around 485.02 and 508.81 cm^{-1}. Moreover, it has been observed that the frequency between 200–1100 for NO@Cu–B_4N_{10}_NC with sharp peaks around 429.12 cm^{-1} (Fig. 5e). Besides, Fig. 5f has exhibited the frequency between 200–1100 for NO@Zn–B_4N_{10}_NC with two sharp peaks around 448.61 and 688.63 cm^{-1}.

Table2. Data of NMR shielding tensors for selected atoms of NO@Sc–B_4N_{10}_NC, NO@V–B_4N_{10}_NC, NO@Cr–B_4N_{10}_NC, NO@Co–B_4N_{10}_NC, NO@Cu–B_4N_{10}_NC, and NO@Zn–B_4N_{10}_NC complexes using CAM–B3LYP–D3/6-311+G(d,p), LANL2DZ calculation.

Sc–B_4N_{10}_NC			V–B_4N_{10}_NC			Cr–B_4N_{10}_NC		
atom	σ_{iso}	σ_{aniso}	atom	σ_{iso}	σ_{aniso}	atom	σ_{iso}	σ_{aniso}
N1	3288.96	12004.50	N1	8364.44	27502.90	N1	657.46	449.15
O2	3784.83	14745.07	O2	18183.11	59763.77	O2	638.05	829.81
B3	45.32	102.76	B3	117.84	562.2156	B3	73.15	59.20
N4	718.03	9476.56	N4	4204.74	19733.21	N4	864.67	935.73
N5	2082.33	7477.11	N5	6249.23	18732.22	N5	663.8211	1162.01
B6	78.50	120.66	B6	178.28	349.74	B6	73.63	64.90
B7	71.78	105.56	B7	160.30	571.58	B7	70.66	58.23
B8	87.30	63.44	B8	139.22	323.74	B8	67.77	55.83
N9	247.05	1130.01	N9	4148.15	10938.01	N9	194.59	867.75
N10	777.90	7170.48	N10	3592.00	14968.85	N10	637.10	1350.34
N11	1036.46	2615.44	N11	5847.52	9357.01	N11	739.01	891.46
N12	722.49	2826.85	N12	1166.50	8750.80	N12	648.83	703.63
N13	1101.54	1740.61	N13	4231.35	9407.75	N13	686.99	715.76
N14	645.32	2891.22	N14	263.18	9470.19	N14	708.80	622.45
Sc15	603.72	722.60	V15	6179.22	3771.37	Cr15	7806.68	2373.72
N16	645.24	4055.32	N16	1944.78	10094.87	N16	309.99	704.31
N17	207.26	6677.00	N17	10575.45	13849.00	N17	1013.79	1526.37
Co–B_4N_{10}_NC			Cu–B_4N_{10}_NC			Zn–B_4N_{10}_NC		
atom	σ_{iso}	σ_{aniso}	atom	σ_{iso}	σ_{aniso}	atom	σ_{iso}	σ_{aniso}
N1	6235.13	21991.86	N1	63293.00	94223.48	N1	1551.16	1716.94
O2	13191.61	46595.00	O2	88823.60	132087.84	O2	1866.55	1659.43
B3	315.80	857.56	B3	31.0022	237.228	B3	59.21	86.06
N4	11531.79	25317.62	N4	3081.29	26445.87	N4	867.69	1132.70
N5	18262.38	59345.21	N5	2474.98	20423.95	N5	80.45	310.76
B6	371.00	784.1426	B6	39.79	210.98	B6	59.63	89.72
B7	322.72	820.1116	B7	66.86	321.73	B7	58.66	84.79
B8	351.29	762.9027	B8	1.84	182.22	B8	58.32	90.12
N9	2775.17	43699.70	N9	1189.16	18670.09	N9	270.49	738.94
N10	16350.09	52405.72	N10	2089.78	23940.52	N10	113.63	385.12
N11	2593.17	5918.10	N11	1208.41	5659.78	N11	913.16	606.23
N12	3290.23	6195.62	N12	4479.93	27757.65	N12	967.93	781.41
N13	653.93	6410.61	N13	2635.56	6052.16	N13	871.75	595.94
N14	1621.05	5288.46	N14	6411.38	25786.03	N14	916.85	656.01
Co15	49289.45	84963.85	Cu15	16157.16	44143.15	Zn15	5.2	431.41
N16	6136.67	43276.78	N16	3203.10	17623.09	N16	273.41	716.23
N17	14002.19	27833.11	N17	8941.76	21869.78	N17	877.54	1156.93
N1	6235.13	21991.86	N1	63293.00	94223.48	N1	1551.16	1716.94

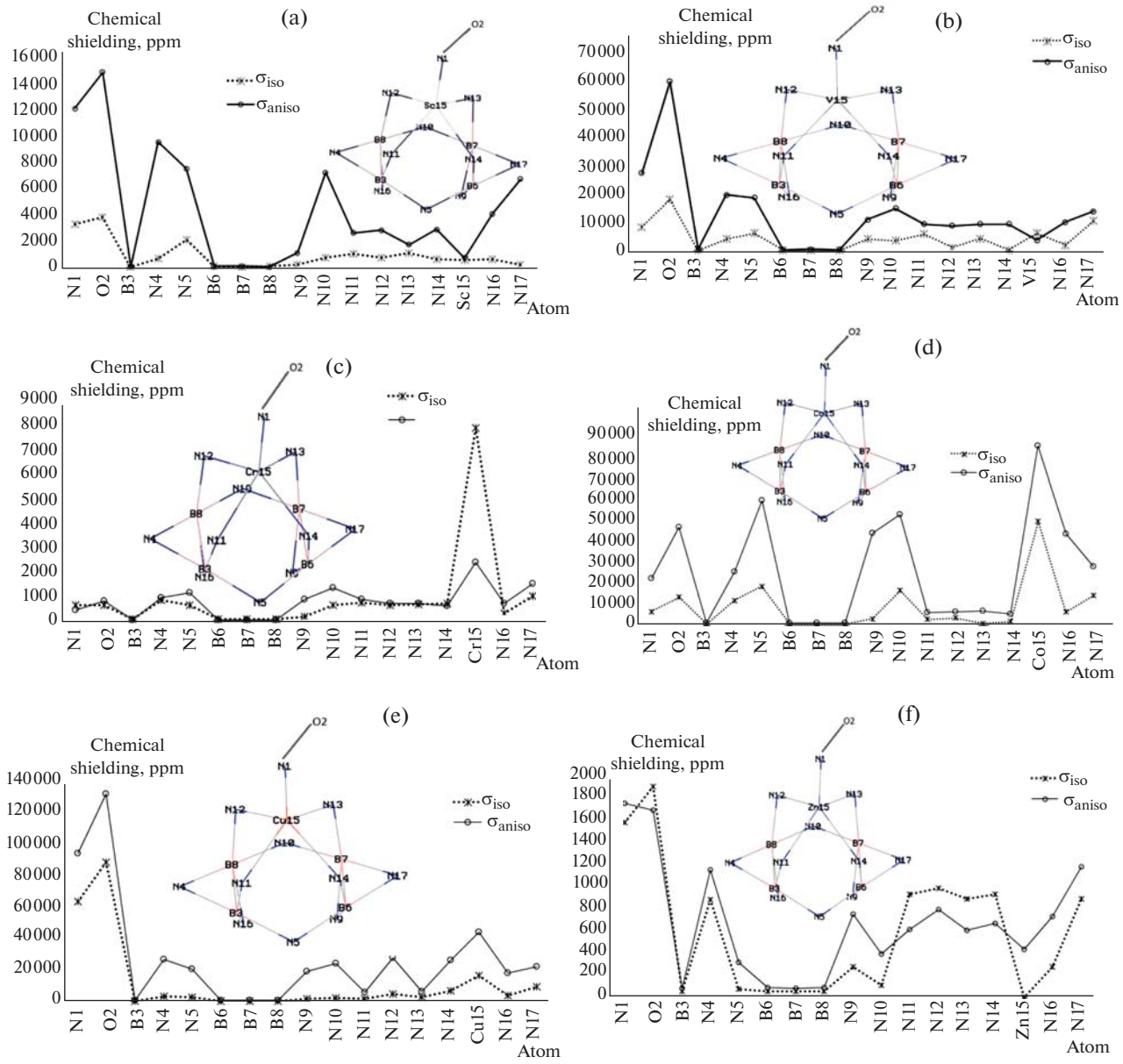

Fig. 4. The NMR spectra for (a) NO@ Sc–B_4N_{10}_NC, (b) NO@V–B_4N_{10}_NC, (c) NO@Cr–B_4N_{10}_NC, (d) NO@Co–B_4N_{10}_NC, (e) NO@Cu–B_4N_{10}_NC, and (f) NO@Zn–B_4N_{10}_NC complexes using CAM–B3LYP–D3/6-311+G(d,p), LANL2DZ.

The IR spectra of NO adsorption on the *X*–B_4N_{10}_NC has demonstrated that the structure of the dominant complex correlates with the electron potency of doped *X* (*X* = Sc, V, Cr, Co, Cu, Zn) on the B_5N_{10}_NC. As it has been seen the doped nanocages of Sc–B_4N_{10}_NC, V–B_4N_{10}_NC, Cr–B_4N_{10}_NC, Co–B_4N_{10}_NC, Cu–B_4N_{10}_NC, and Zn–B_4N_{10}_NC complexes have the most fluctuations and the highest tendency for adsorption of NO around 450 cm^{-1}. Therefore, it can be found that IR spectroscopy of NO-adsorbed *X*–B_4N_{10}_NC is now well-placed to address specific questions on the individual effect of charge carriers (gas molecule-nanocage), as well as doping atoms on the overall structure (Figs. 5a–5f).

Table 3 through the thermodynamic specifications concluded that *X*–B_4N_{10}_NC due to adsorption of NO might be more efficient sensors for detecting and removing the gas molecules from the polluted air.

Thermodynamic parameters of NO gas molecules adsorption on the *X*–B_4N_{10}_NC have been deter-

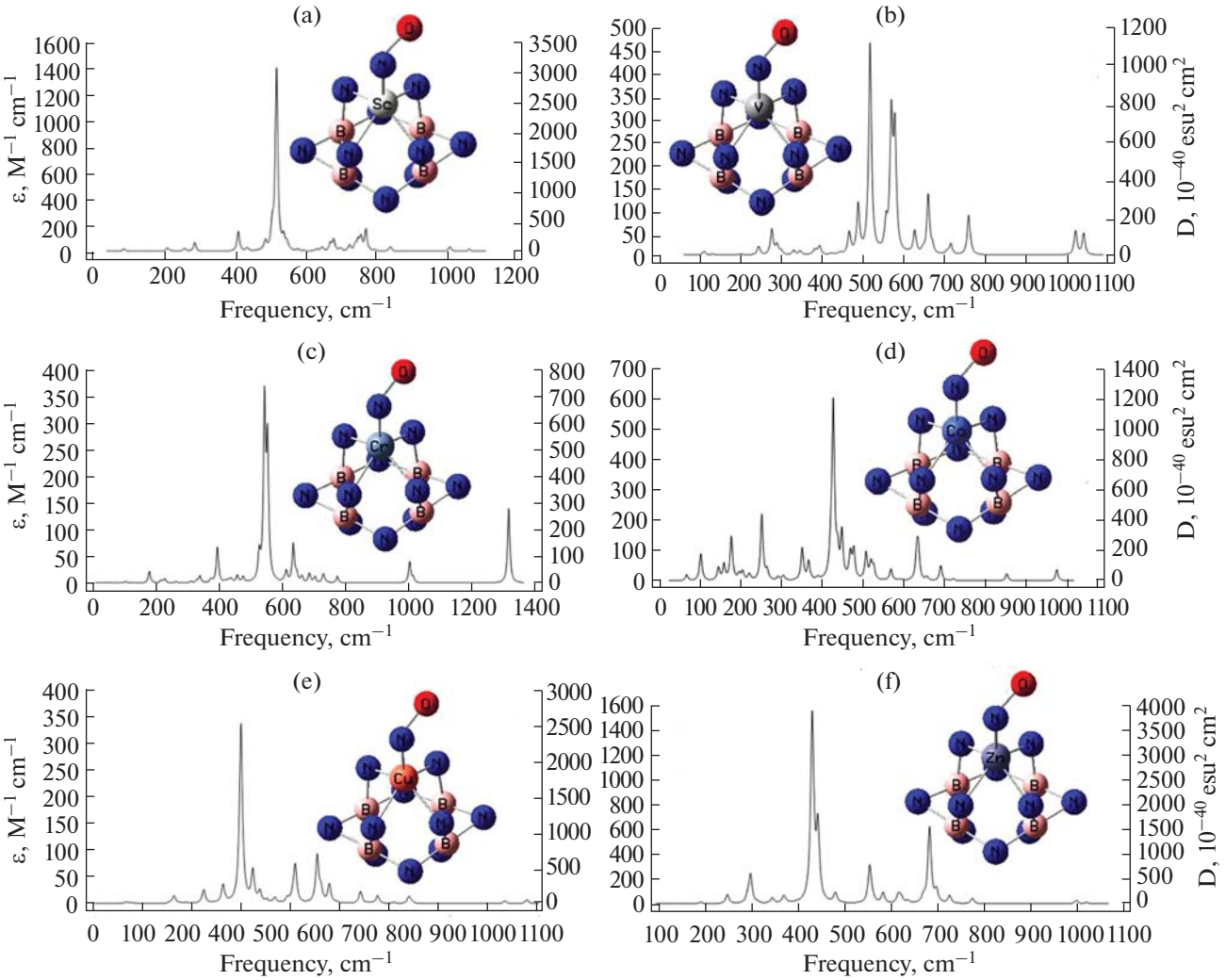

Fig. 5. The Frequency (cm^{-1}) changes through the IR spectra for (a) NO@Sc–B_4N_{10}_NC, (b) NO@V–B_4N_{10}_NC, (c) NO@Cr–B_4N_{10}_NC, (d) NO@Co–B_4N_{10}_NC, (e) NO@Cu–B_4N_{10}_NC, and (f) NO@Zn–B_4N_{10}_NC complexes using CAM–B3LYP–D3/6-311+G(d,p), LANL2DZ.

mined using DFT theoretical technique. It has been shown that for a given number of nitrogen donor sites in NO, the stabilities of complexes owing to doping atoms of Sc, V, Cr, Co, Cu, Zn can be considered as: NO@Cu–B_4N_{10}_NC ⩾ NO@Co–B_4N_{10}_NC > NO@Cr–B_4N_{10}_NC > NO@V–B_4N_{10}_NC > NO@Zn–B_4N_{10}_NC > NO@Sc–B_4N_{10}_NC (Table 3).

The thermodynamic data in Fig. 6 could detect the maximum efficiency of Sc, V, Cr, Co, Cu, Zn atoms doping of B_5N_{10}_NC for gas molecules adsorption through ΔG_R° which depends on the covalent bond between NO gas molecules and X–B_4N_{10}_NC as a potent sensor for air pollution removal.

The adsorption process of NO gas molecules on the X–B_4N_{10}_NC is affirmed by the ΔG_{ads}° quantities:

$$\Delta G_{ads}^\circ = \Delta G_{NO@X-B4N10\_NC}^\circ - \left(\Delta G_{NO}^\circ + \Delta G_{X-B4N10\_NC}^\circ\right); \quad (11)$$

Sc,V,Cr,Co, Cu, Zn.

Figure 6 has shown that the key role of doped atoms of Sc, V, Cr, Co, Cu, Zn during interaction between the adsorbates of NO gas molecules as the electron donors and the adsorbent of Sc–B_4N_{10}_NC, V–B_4N_{10}_NC, Cr–B_4N_{10}_NC, Co–B_4N_{10}_NC, Cu–B_4N_{10}_NC, and Zn–B_4N_{10}_NC as electron acceptors. Therefore, the selectivity of atom-doped on boron nitride nanocage (gas sensor) for gas molecules adsorption can be resulted as: Cu ⩾ Co > Cr > V > Zn > Sc (Table 3 and Fig. 6).

Table 3. The thermodynamic characters of NO@Sc–B_4N_{10}_NC, NO@V–B_4N_{10}_NC, NO@Cr–B_4N_{10}_NC, NO@Co–B_4N_{10}_NC, NO@Cu–B_4N_{10}_NC, and NO@Zn–B_4N_{10}_NC complexes using CAM–B3LYP–D3/6-311+G(d,p), LANL2DZ calculation

Compound	$\Delta E° \times 10^{-3}$, kcal/mol	$\Delta H° \times 10^{-3}$, kcal/mol	$\Delta G° \times 10^{-3}$, kcal/mol	$S°$, cal/K mol	Dipole moment, D
NO@Sc–B_4N_{10}_NC	–515.659	–515.659	–515.688	100.315	0.9301
NO@V–B_4N_{10}_NC	–531.306	–531.306	–531.337	105.216	0.3502
NO@Cr–B_4N_{10}_NC	–540.960	–540.959	–540.993	111.987	0.7802
NO@Co–B_4N_{10}_NC	–577.471	–577.471	–577.503	109.405	0.5716
NO@Cu–B_4N_{10}_NC	–609.782	–609.781	–609.813	106.275	0.4199
NO@Zn–B_4N_{10}_NC	–527.877	–527.876	–527.907	103.769	0.5630

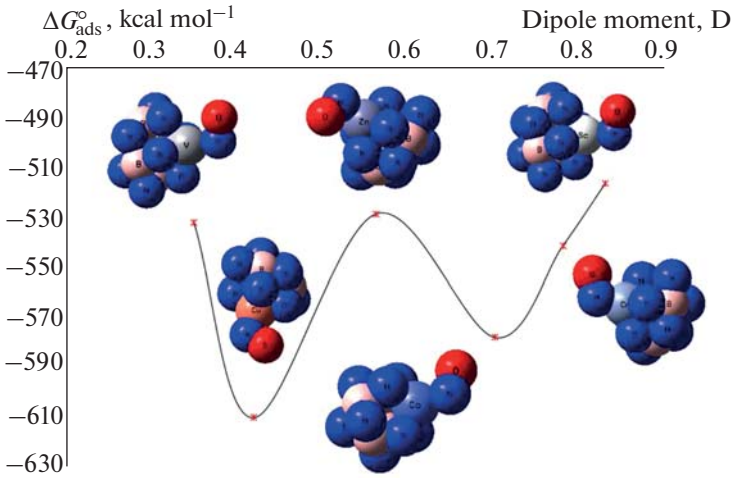

Fig. 6. Gibbs free energy ($\Delta G°_R$) versus dipole moment (D) for NO@Sc–B_4N_{10}_NC, NO@V–B_4N_{10}_NC, NO@Cr–B_4N_{10}_NC, NO@Co–B_4N_{10}_NC, NO@Cu–B_4N_{10}_NC, and NO@Zn–B_4N_{10}_NC complexes using CAM–B3LYP–D3/6-311+G(d,p), LANL2DZ calculation.

4. CONCLUSIONS

This research has investigated doping of Sc, V, Cr, Co, Cu, Zn transition metals on the boron nitride nanocage (X–B_4N_{10}_NC) for enhancing toxic gas sensing of these nanomaterials for air pollution removal. Therefore, NO gas molecules separation involving the X–B_4N_{10}_NC has been experimented based on electrostatic interactions between the gas molecules and X–B_4N_{10}_NC.

The electromagnetic and thermodynamic properties of X–B_4N_{10}_NC complexes were computed using density functional theory. The results have illustrated that chosen gas molecules adsorbed on the X–B_4N_{10}_NC are rather stable with the most stable adsorption site being in the center of X–B_4N_{10}_NC system. The selectivity of atom-doped on boron nitride nanocage (gas sensor) for gas molecules adsorption can be resulted as: NO@Cu–B_4N_{10}_NC ⩾ NO@Co–B_4N_{10}_NC > NO@Cr–B_4N_{10}_NC > NO@V–B_4N_{10}_NC > NO@Zn–B_4N_{10}_NC > NO@Sc–B_4N_{10}_NC, respectively.

This work proposes that transition metals as ferromagnetic semiconductors can be examined through doping on the nanomaterials for enhancing the adsorption potency towards designing the pollution removal sensors.

ACKNOWLEDGMENTS

In successfully completing this paper and its research, the author is grateful to Kastamonu University.

AUTHOR CONTRIBUTION

Conceptualization and idea, methodology, software, validation, formal analysis, investigation, data curation, writing-original draft preparation, visualization, supervision, project administration, writing-review and editing, resources.

FUNDING

This work was supported by ongoing institutional funding. No additional grants to carry out or direct this particular research were obtained.

CONFLICT OF INTEREST

The author of this work declares that he has no conflicts of interest.

REFERENCES

1. Gonzalez-Ortiz, D., Salameh, C., Bechelany, M., and Miele, P., Nanostructured boron nitride-based materials: Synthesis and applications, *Mater. Today Adv.*, 2020, vol. 8, p. 100107. https://doi.org/10.1016/j.mtadv.2020.100107
2. Mishra, N.S. and Saravanan, P., A review on the synergistic features of hexagonal boron nitride (white graphene) as adsorbent-photo active nanomaterial, *ChemistrySelect*, 2018, vol. 3, no. 28, pp. 8023–8034. https://doi.org/10.1002/slct.201801524
3. Weng, Q., Wang, X., Wang, X., Bando, Yo., and Golberg, D., Functionalized hexagonal boron nitride nanomaterials: Emerging properties and applications, *Chem. Soc. Rev.*, 2016, vol. 45, no. 14, pp. 3989–4012. https://doi.org/10.1039/c5cs00869g
4. Delia, A., Muñoz, O., Escobedo-Morales, A., Skakerzadeh, E., and Anota, E.Ch., Effect of homonuclear boron bonds in the adsorption of DNA nucleobases on boron nitride nanosheets, *J. Mol. Liq.*, 2021, vol. 322, p. 114951. https://doi.org/10.1016/j.molliq.2020.114951
5. Shtansky, D.V., Matveev, A.T., Permyakova, E.S., Leybo, D.V., Konopatsky, A.S., and Sorokin, P.B., Recent progress in fabrication and application of BN nanostructures and BN-based nanohybrids, *Nanomaterials*, 2022, vol. 12, no. 16, p. 2810. https://doi.org/10.3390/nano12162810
6. Yang, Yu., Peng, Yi., Saleem, M.F., Chen, Z., and Sun, W., Hexagonal boron nitride on III–V compounds: A review of the synthesis and applications, *Materials*, 2022, vol. 15, no. 13, p. 4396. https://doi.org/10.3390/ma15134396
7. Davies, A., Albar, J.D., Summerfield, A., Thomas, J.C., Cheng, T.S., Korolkov, V.V., Stapleton, E., Wrigley, J., Goodey, N.L., Mellor, Ch.J., Khlobystov, A.N., Watanabe, K., Taniguchi, T., Foxon, C.T., Eaves, L., Novikov, S.V., and Beton, P.H., Lattice-matched epitaxial graphene grown on boron nitride, *Nano Lett.*, 2018, vol. 18, no. 1, pp. 498–504. https://doi.org/10.1021/acs.nanolett.7b04453
8. Bangari, R.S., Yadav, V.K., Singh, J.K., and Sinha, N., Fe_3O_4-functionalized boron nitride nanosheets as novel adsorbents for removal of arsenic(III) from contaminated water, *ACS Omega*, 2020, vol. 5, no. 18, pp. 10301–10314. https://doi.org/10.1021/acsomega.9b04295
9. Chao, Ya., Zhang, J., Li, H., Wu, P., Li, X., Chang, H., He, J., Wu, H., Li, H., and Zhu, W., Synthesis of boron nitride nanosheets with N-defects for efficient tetracycline antibiotics adsorptive removal, *Chem. Eng. J.*, 2020, vol. 387, p. 124138. https://doi.org/10.1016/j.cej.2020.124138
10. Vatanpour, V., Mehrabani, S.A.N., Keskin, B., Arabi, N., Zeytuncu, B., and Koyuncu, I., A comprehensive review on the applications of boron nitride nanomaterials in membrane fabrication and modification, *Ind. Eng. Chem. Res.*, 2021, vol. 60, no. 37, pp. 13391–13424.
11. Larki, S., Shakerzadeh, E., Anota, E.Ch., and Behjatmanesh-Ardakani, R., The Al, Ga and Sc dopants effect on the adsorption performance of $B_{12}N_{12}$ nanocluster toward pnictogen hydrides, *Chem. Phys.*, 2019, vol. 526, p. 110424. https://doi.org/10.1016/j.chemphys.2019.110424
12. Guo, Yo., Wang, R., Wang, P., Rao, L., and Wang, Ch., Developing a novel layered boron nitride–carbon nitride composite with high efficiency and selectivity to remove protonated dyes from water, *ACS Sustainable Chem. Eng.*, 2019, vol. 7, no. 6, pp. 5727–5741. https://doi.org/10.1021/acssuschemeng.8b05150
13. Henkelman, G., Arnaldsson, A., and Jónsson, H., A fast and robust algorithm for Bader decomposition of charge density, *Comput. Mater. Sci.*, 2006, vol. 36, no. 3, pp. 354–360. https://doi.org/10.1016/j.commatsci.2005.04.010
14. Blöchl, P.E., Projector augmented-wave method, *Phys. Rev. B*, 1994, vol. 50, no. 24, pp. 17953–17979. https://doi.org/10.1103/physrevb.50.17953
15. Perdew, J.P., Burke, K., and Ernzerhof, M., Generalized gradient approximation made simple, *Phys. Rev. Lett.*, 1996, vol. 77, no. 18, pp. 3865–3868. https://doi.org/10.1103/physrevlett.77.3865
16. Ziesche, P., Kurth, S., and Perdew, J.P., Density functionals from LDA to GGA, *Comput. Mater. Sci.*, 1998, vol. 11, no. 2, pp. 122–127. https://doi.org/10.1016/s0927-0256(97)00206-1
17. Arrigoni, M. and Madsen, G.K.H., Comparing the performance of LDA and GGA functionals in predicting the lattice thermal conductivity of III–V semiconductor materials in the zincblende structure: The cases of AlAs and BAs, *Comput. Mater. Sci.*, 2019, vol. 156, pp. 354–360. https://doi.org/10.1016/j.commatsci.2018.10.005
18. Hohenberg, P. and Kohn, W., Inhomogeneous electron gas, *Phys. Rev.*, 1964, vol. 136, no. 3b, pp. b864–b871. https://doi.org/10.1103/physrev.136.b864
19. Kohn, W. and Sham, L.J., Self-consistent equations including exchange and correlation effects, *Phys. Rev.*, 1965, vol. 140, no. 4a, pp. a1133–a1138. https://doi.org/10.1103/physrev.140.a1133
20. Becke, A.D., Density-functional thermochemistry. III. The role of exact exchange, *J. Chem. Phys.*, 1993, vol. 98, no. 7, pp. 5648–5652. https://doi.org/10.1063/1.464913
21. Lee, Ch., Yang, W., and Parr, R.G., Development of the Colle–Salvetti correlation-energy formula into a functional of the electron density, *Phys. Rev. B*, 1988, vol. 37, no. 2, pp. 785–789. https://doi.org/10.1103/physrevb.37.785
22. Kim, K. and Jordan, K.D., Comparison of density functional and MP2 calculations on the water monomer and dimer, *J. Phys. Chem.*, 1994, vol. 98, no. 40,

pp. 10089–10094.
https://doi.org/10.1021/j100091a024

23. Stephens, P.J., Devlin, F.J., Chabalowski, C.F., and Frisch, M.J., Ab initio calculation of vibrational absorption and circular dichroism spectra using density functional force fields, *J. Phys. Chem.*, 1994, vol. 98, no. 45, pp. 11623–11627.
https://doi.org/10.1021/j100096a001

24. Cramer, C.J., *Essentials of Computational Chemistry: Theories and Models*, Chichester: Wiley, 2004, 2nd ed.

25. Mollaamin, F. and Monajjemi, M., Corrosion inhibiting by some organic heterocyclic inhibitors through langmuir adsorption mechanism on the Al–X (X = Mg/Ga/Si) alloy surface: A study of quantum three-layer method of CAM-DFT/ONIOM, *J. Bio- Tribo-Corros.*, 2023, vol. 9, no. 2, p. 33.
https://doi.org/10.1007/s40735-023-00751-y

26. Mollaamin, F. and Monajjemi, M., Molecular modelling framework of metal–organic clusters for conserving surfaces: Langmuir sorption through the TD-DFT/ONIOM approach, *Mol. Simul.*, 2023, vol. 49, no. 4, pp. 365–376.
https://doi.org/10.1080/08927022.2022.2159996

27. Vosko, S.H., Wilk, L., and Nusair, M., Accurate spin-dependent electron liquid correlation energies for local spin density calculations: A critical analysis, *Can. J. Phys.*, 1980, vol. 58, no. 8, pp. 1200–1211.
https://doi.org/10.1139/p80-159

28. Frisch, M.J., Trucks, G.W., Schlegel, H.B., Scuseria, G.E., Robb, M.A., et al., *Gaussian 16, Revision C.01*, Wallingford, CT: Gaussian, 2016.

29. Dennington, R., Keith, T.A., and Millam, J.M., *GaussView, Version 6.06.16*, Shawnee Mission, KS: Semichem, 2016.

30. Smith, J.A.S., Nuclear quadrupole resonance spectroscopy. General principles, *J. Chem. Educ.*, 1971, vol. 48, no. 1, pp. 39–41.
https://doi.org/10.1021/ed048p39

31. Garroway, A.N. (Naval Research Laboratory), Nuclear quadrupole resonance, *Alternatives for Landmine Detection. Report MR-1608*, MacDonald, J. and Lockwood, J.R., Eds., Rand Corporation, 2003.

32. Poleshchuk, O.Kh., Kalinina, E.L., Latosińska, J.N., and Koput, J., Application of density functional theory to the analysis of electronic structure and quadrupole interaction in dimers of transition and non-transition elements, *J. Mol. Struct.: THEOCHEM*, 2001, vol. 574, nos. 1–3, pp. 233–243.
https://doi.org/10.1016/s0166-1280(01)00636-4

33. Young, H.A. and Freedman, R.D., *Sears and Zemansky's University Physics: With Modern Physics*, Boston: Addison-Wesley, 2012, 13th ed.

34. Sohail, U., Ullah, F., Binti Zainal Arfan, N.H., Abdul Hamid, M.H.Sh., Mahmood, T., Sheikh, N.S., and Ayub, Kh., Transition metal sensing with nitrogenated holey graphene: A first-principles investigation, *Molecules*, 2023, vol. 28, no. 10, p. 4060.
https://doi.org/10.3390/molecules28104060